Automatica 178 (2025) 112351

Contents lists available at ScienceDirect

Automatica

journal homepage: www.elsevier.com/locate/automatica

Brief paper

Backstepping neural operators for 2×2 hyperbolic PDEs[☆]

Shanshan Wang [a], Mamadou Diagne [b,*], Miroslav Krstic [b]

[a] Department of Control Science and Engineering, University of Shanghai for Science and Technology, Shanghai, 200093, PR China
[b] Department of Mechanical and Aerospace Engineering, University of California San Diego, La Jolla, CA, 92093, USA

ARTICLE INFO

Article history:
Received 22 January 2024
Received in revised form 23 December 2024
Accepted 8 April 2025

Keywords:
PDE backstepping
Deep learning
Neural networks
Distributed parameter systems

ABSTRACT

Deep neural network approximation of nonlinear operators, commonly referred to as DeepONet, has proven capable of approximating PDE backstepping designs in which a single Goursat-form PDE governs a single feedback gain function. In boundary control of coupled hyperbolic PDEs, coupled Goursat-form PDEs govern two or more gain kernels — a structure unaddressed thus far with DeepONet. In this contribution, we open the subject of approximating systems of gain kernel PDEs by considering a counter-convecting 2×2 hyperbolic system whose backstepping boundary controller and observer gains are the solutions to 2×2 kernel PDE systems in Goursat form. We establish the continuity of the mapping from (a total of five) functional coefficients of the plant to the kernel PDEs solutions, prove the existence of an arbitrarily close DeepONet approximation to the kernel PDEs, and ensure that the DeepONet-based approximated gains guarantee stabilization when replacing the exact backstepping gain kernel functions. Taking into account anti-collocated boundary actuation and sensing, our L^2*-globally-exponentially stabilizing (GES)* control law requires the deep learning of both the controller and the observer gains. Moreover, the encoding of the feedback law into DeepONet ensures *semi-global practical exponential stability (SG-PES),* as established in our result. The neural operators (NOs) speed up the computation of both controller and observer gains by multiple orders of magnitude. Its theoretically proved stabilizing capability is demonstrated through simulations.

1. Introduction

Coupled first-order hyperbolic PDE systems are versatile, finding applications in traffic dynamics (Goatin, 2006; Yu & Krstic, 2019) and open channel fluid flow (Diagne, Bastin, & Coron, 2012; Diagne, Diagne, Tang, & Krstic, 2017; Diagne, Tang, Diagne, & Krstic, 2017; Halleux, Prieur, Coron, D'Andrea-Novel, & Bastin, 2003; Somathilake & Diagne, 2024), to name a few. The development of stabilizing boundary feedback laws for such systems began with the locally exponentially stabilizing boundary controller in Coron, D'Andrea-Novel, and Bastin (1999), crafted for the Saint-Venant model. This controller used an entropy-based Lyapunov function to exponentially stabilize a system where total energy was not a suitable Lyapunov candidate. Subsequent works utilized the Riemann invariants method for exponential stability using local water level measurements at gates without friction. Key contributions in Bastin and Coron (2010, 2011), and Vazquez, Krstic, and Coron (2011) led to a quadratic Lyapunov candidate for 2×2 linear hyperbolic systems. Our work focuses on the PDE backstepping approach, using a single boundary actuation and observer-based design as in Vazquez et al. (2011) (refer to Vazquez, Coron, Krstic, & Bastin, 2012 for the quasilinear case). The "dissipativity" method from Bastin and Coron (2010, 2011) is an observer-free approach that involves finding dissipative boundary conditions akin to "small gain conditions," relying on dual boundary actuation and measurements at gate locations. Leveraging Marcum Q-functions, explicit kernels for the stabilization of 2×2 linear hyperbolic systems with constant coefficients are derived in Vazquez and Krstic (2014). Recently, delay-adaptive boundary control of coupled hyperbolic PDE-ODE cascade systems was established via Batch-Least Square Identification (BaLSI) (Karafyllis, Kontorinaki, & Krstic, 2020; Wang & Diagne, 2024). PDE backstepping has been used to control a $2+1$ counter-convective system actuated at one boundary (Burkhardt, Yu, & Krstic, 2021; Di Meglio, Vazquez, Krstic, & Petit, 2012). The problem structure outlined in Di Meglio, Kaasa, Petit, and Alstad (2012) has broad applicability, appearing in various multiphase flow of coupled water-sediment dynamics in river breaches (Diagne, Diagne, et al., 2017), where exponential stabilization of supercritical flow regimes, has been achieved, which was not attainable applying the design proposed in Diagne et al. (2012).

☆ The full-state feedback design was presented at the 2024 American Control Conference (ACC), July 10- July 12, 2023, Toronto, ON, Canada. This paper was recommended for publication in revised form by Associate Editor Anton Selivanov under the direction of Editor Florian Dorfler.

* Corresponding author.
E-mail addresses: shanshanwang@usst.edu.cn (S. Wang), mdiagne@ucsd.edu (M. Diagne), krstic@ucsd.edu (M. Krstic).

https://doi.org/10.1016/j.automatica.2025.112351
0005-1098/

Generalized results on the exponential stabilization of an arbitrary number of coupled waves were achieved in Di Meglio, Vazquez, and Krstic (2013) and Hu, Di Meglio, Vazquez, and Krstic (2016) as non-trivial extensions of Di Meglio, Vazquez, et al. (2012) and Vazquez et al. (2011) to the so-called $n+1$ and $n+m$ cases. Following these major developments, Anfinsen, Diagne, Aamo, and Krstic (2016) and Anfinsen, Diagne, Aamo, and Krstic (2017) proposed adaptive observers to estimate boundary parameters of both $n+1$ and $n+m$ systems motivated by the identification of the bottom hole influxes of hydrocarbon caused by high-pressure formations in the well during oil drilling operations. These developments were followed by major progress on adaptive control design (Anfinsen & Aamo, 2019).

In general, the conception of PDE controllers can lead to complex gain functions that require non-obvious computational effort. Our contribution signifies advancement in leveraging the computational capabilities offered by Machine Learning techniques to enhance the feasibility of hyperbolic PDE control.

Contributions: We expedite the computation of gain kernel PDEs arising in the context of backstepping control design for coupled hyperbolic systems. Developing further the DeepONet design originally introduced in Bhan, Shi, and Krstic (2024b) and then Krstic, Bhan, and Shi (2024) and Qi, Zhang, and Krstic (2024) for simpler PDE systems, we introduce Neural Operator (NO) approximations for kernels applicable to 2×2 hyperbolic PDEs to encapsulate the mapping from the functional coefficients of the plant into a previously trained DeepONet. We design a neural network architecture, more precisely, a computational resource capable of calculating the gains through function evaluations, eliminating the necessity to solve the coupled gain kernel PDEs defined on a triangular domain. Recently, DeepONet achieved gain kernels computation for full-state feedback control in ARZ traffic system in Zhang, Zhong, and Yu (2024). Furthermore, results on DeepONet-based adaptive control (Lamarque, Bhan, Shi, & Krstic, 2025), gain scheduling (Lamarque, Bhan, Vazquez, & Krstic, 2025) and moving-horizon estimators (MHE) (Bhan, Shi, Karafyllis, Krstic, Rawlings, 2024a) were recently developed.

Differing from Wang, Diagne, and Krstic (2025), where DeepONet approximation of gain kernel PDEs was achieved using a composition of operators defined by a single hyperbolic PDE in Goursat form and one parabolic PDE defined in a rectangular domain, the scenario involving coupled hyperbolic PDEs in cascade, along with the observer state, results in the DeepONet approximation of gain kernel functions governed by a pair of coupled hyperbolic PDEs in Goursat form. Two of these PDEs originate from the controller, while the other two are the observer gain kernel PDEs. The controller and observer gains approximated via DeepONet are the outputs of a pair of 2×2 nonlinear operators of Goursat PDEs "powered" by five functional coefficients of the plant. The structure of the studied DeepONet of nonlinear operators broadens the scope of neural operators design originally introduced by the machine learning community (Lu, Jin, & Karniadakis, 2019). Our contribution is twofold:

- **DeepONet for the gain kernels of the output-feedback law.** We derive a *global exponential stability (GES)* result for a coupled hyperbolic system equipped with an output feedback control law informed by the NO-based approximated controller and observer gain kernel functions. Because the controller-observer system is a composition of two linear systems, the global exponential stability is preserved.
- **DeepONet for the fully learned output feedback law.** Leveraging insights from the DeepONet approximations of both the controller–observer gain kernels and the observed system states, we develop NO approximation for the output-feedback control law, incorporating the observer state. This method fully learns the control law for a 2×2 hyperbolic system using anti-collocated boundary actuation and sensing. We establish a *semi-global practical exponential stability (SG-PES)* estimate for the closed-loop system. This SG-PES result stems from approximating the Goursat-form PDEs and observer states $\hat{u}$ and $\hat{v}$, resulting in both multiplicative and additive approximation errors. The stability is semi-global as the dataset includes bounded samples of observer states $\hat{u}$ and $\hat{v}$.

In the nutshell, our approach significantly accelerates the computation of both controller and observer gains. Our theoretically established stability results are illustrated by simulation results and the code is available at github.

Organization of the paper: Section 2 succinctly presents the design of an exponentially stabilizing output-feedback boundary control law for 2×2 hyperbolic systems. Sections 3 and 4 present the approximation of the kernel operators and the global exponential stabilization (GES) under the approximated controller gain functions and observer gain functions via DeepONet. Section 5 presents a semi-global practical exponential stability (SG-PES) result when the totality of the output feedback law is learned via DeepONet. Section 6 and Section 7 present simulation results and concluding remarks, respectively.

Notation: We define the L^2-norm for $\chi(x) \in L^2[0,1]$ as $\|\chi\|_{L^2}^2 = \int_0^1 |\chi(x)|^2 dx$. For the convenience, we set $\|\chi\|^2 = \|\chi\|_{L^2}^2$. The supremum norm is denoted $\|\cdot\|_\infty$.

2. Preliminaries and problem statement

Preliminaries. We consider linear hyperbolic systems

$$\partial_t u(x,t) = -\lambda(x)\partial_x u(x,t) + \sigma(x)u(x,t) + \omega(x)v(x,t), \tag{1}$$

$$\partial_t v(x,t) = \mu(x)\partial_x v(x,t) + \theta(x)u(x,t), \tag{2}$$

with boundary conditions

$$u(0,t) = qv(0,t), \quad v(1,t) = U(t), \tag{3}$$

where, $\lambda,\mu \in C^1([0,1])$, $\sigma,\omega,\theta \in C^0([0,1])$, $q\in\mathbb{R}$, and initial conditions $v^0(x)$, $u^0(x) \in L^2([0,1])$. The transport speeds are assumed to satisfy $-\mu(x) < 0 < \lambda(x)$, $\forall x \in [0,1]$, and λ, μ, σ, ω, θ are all bounded with $\underline{\lambda} \le \lambda \le \bar{\lambda}$, $\underline{\mu} \le \mu \le \bar{\mu}$, $\underline{\sigma} \le \sigma \le \bar{\sigma}$, $\underline{\omega} \le \omega \le \bar{\omega}$, and $\underline{\theta} \le \theta \le \bar{\theta}$.

2.1. Full-state boundary feedback control law

Exploiting the following backstepping transformation (Di Meglio et al., 2013),

$$\beta(x,t) = v(x,t) - \int_0^x k_1(x,\xi)u(\xi,t)d\xi - \int_0^x k_2(x,\xi)v(\xi,t)d\xi, \tag{4}$$

system (1)–(3) is transformed into the target system

$$\begin{aligned}\partial_t u(x,t) &= -\lambda(x)\partial_x u(x,t) + \sigma(x)u(x,t) + \omega(x)\beta(x,t)\\ &\quad + \int_0^x c(x,\xi)u(\xi,t)d\xi + \int_0^x \kappa(x,\xi)\beta(\xi,t)d\xi,\end{aligned} \tag{5}$$

$$\partial_t \beta(x,t) = \mu(x)\partial_x \beta(x,t), \tag{6}$$

with boundary conditions defined as

$$u(0,t) = q\beta(0,t), \quad \beta(1,t) = 0, \tag{7}$$

where $c(x,\xi)$ and $\kappa(x,\xi)$ are functions to be determined. The realization of this mapping requires the kernels in the backstepping transformation (4) to satisfy the following PDEs[1]

$$\mu(x)\partial_x k_1 - \lambda(\xi)\partial_\xi k_1 = \lambda'(\xi)k_1 + \sigma(\xi)k_1 + \theta(\xi)k_2, \tag{8}$$

$$\mu(x)\partial_x k_2 + \mu(\xi)\partial_\xi k_2 = -\mu'(\xi)k_2 + \omega(\xi)k_1, \tag{9}$$

with boundary conditions

$$k_1(x,x) = -\frac{\theta(x)}{\lambda(x)+\mu(x)}, \tag{10}$$

$$\mu(0)k_2(x,0) = q\lambda(0)k_1(x,0). \tag{11}$$

The system (8)–(11) defined over the triangular domain $\mathcal{T} = \{(x,\xi) \mid 0 \le \xi \le x \le 1\}$, is a coupled 2×2 Goursat PDE system that governs the two gain kernels and the coefficient κ and c are chosen to satisfy

$$\kappa(x,\xi) = \omega(x)k_2(x,\xi) + \int_\xi^x \kappa(x,s)k_2(s,\xi)ds, \tag{12}$$

$$c(x,\xi) = \omega(x)k_1(x,\xi) + \int_\xi^x \kappa(x,s)k_1(s,\xi)ds. \tag{13}$$

From (3), (4), and (7), the boundary controller is

$$U(t) = \int_0^1 k_1(1,\xi)u(\xi,t)d\xi + \int_0^1 k_2(1,\xi)v(\xi,t)d\xi. \tag{14}$$

The invertibility of the transformation (4) together with the existence of a unique solution to (8)–(11) was established in Di Meglio et al. (2013). The invertibility of the transformation induces equivalent stability properties of the target and original systems.

The inverse transformation of (4) is given by

$$v(x,t) = \beta(x,t) + \int_0^x l_1(x,\xi)u(\xi,t)d\xi + \int_0^x l_2(x,\xi)\beta(\xi,t)d\xi, \tag{15}$$

where

$$l_1(x,\xi) = k_1(x,\xi) + \int_\xi^x k_2(x,s)l_1(s,\xi)ds, \tag{16}$$

$$l_2(x,\xi) = k_2(x,\xi) + \int_\xi^x k_2(x,s)l_2(s,\xi)ds. \tag{17}$$

2.2. Observer design for an output feedback control law

In this section, we present the design of an exponentially convergent observer capable of estimating the spatially distributed states of system (1)–(3) using the available boundary point measurement $v(0,t)$, which is anti-collocated with the boundary point of actuation. The following backstepping observer is designed:

$$\partial_t\hat{u}(x,t) = -\lambda(x)\partial_x\hat{u}(x,t) + \sigma(x)\hat{u}(x,t) + \omega(x)\hat{v}(x,t) + p_1(x)(v(0,t) - \hat{v}(0,t)), \tag{18}$$

$$\partial_t\hat{v}(x,t) = \mu(x)\partial_x\hat{v}(x,t) + \theta(x)\hat{u}(x,t) + p_2(x)(v(0,t) - \hat{v}(0,t)), \tag{19}$$

with boundary conditions

$$\hat{u}(0,t) = qv(0,t), \quad \hat{v}(1,t) = U(t). \tag{20}$$

The functions $p_1(x)$ and $p_2(x)$ are the observer output injection gains given later. Denoting the observer error likes $\tilde{u}(x,t) = u(x,t) - \hat{u}(x,t)$, it follows the error dynamics

$$\partial_t\tilde{u}(x,t) = -\lambda(x)\partial_x\tilde{u}(x,t) + \sigma(x)\tilde{u}(x,t) + \omega(x)\tilde{v}(x,t) - p_1(x)\tilde{v}(0,t), \tag{21}$$

$$\partial_t\tilde{v}(x,t) = \mu(x)\partial_x\tilde{v}(x,t) + \theta(x)\tilde{u}(x,t) - p_2(x)\tilde{v}(0,t), \tag{22}$$

with boundary conditions

$$\tilde{u}(0,t) = 0, \quad \tilde{v}(1,t) = 0. \tag{23}$$

To design the observer output injection gains, backstepping transformations are again introduced as

$$\tilde{u}(x,t) = \tilde{\alpha}(x,t) + \int_0^x m_1(x,\xi)\tilde{\beta}(\xi,t)d\xi, \tag{24}$$

$$\tilde{v}(x,t) = \tilde{\beta}(x,t) + \int_0^x m_2(x,\xi)\tilde{\beta}(\xi,t)d\xi, \tag{25}$$

to map system (21)–(23) into the target system

$$\partial_t\tilde{\alpha}(x,t) = -\lambda(x)\partial_x\tilde{\alpha}(x,t) + \sigma(x)\tilde{\alpha}(x,t) + \int_0^x g(x,\xi)\tilde{\alpha}(\xi,t)d\xi, \tag{26}$$

$$\partial_t\tilde{\beta}(x,t) = \mu(x)\partial_x\tilde{\beta}(x,t) + \theta(x)\tilde{\alpha}(x,t) + \int_0^x h(x,\xi)\tilde{\alpha}(\xi,t)d\xi, \tag{27}$$

with boundary conditions

$$\tilde{\alpha}(0,t) = 0, \quad \tilde{\beta}(1,t) = 0, \tag{28}$$

where $g(x,\xi)$ and $h(x,\xi)$ are given below

$$g(x,\xi) = -\theta(\xi)m_1(x,\xi) - \int_\xi^x m_1(x,s)h(s,\xi)ds, \tag{29}$$

$$h(x,\xi) = -\theta(\xi)m_2(x,\xi) - \int_\xi^x m_2(x,s)h(s,\xi)ds. \tag{30}$$

Following Di Meglio et al. (2013), the mapping of (21)–(23) to (26)–(28), requires the kernels of (24) and (25) to satisfy

$$\lambda(x)\partial_x m_1 - \mu(\xi)\partial_\xi m_1 = \mu'(\xi)m_1 + \delta(x)m_1 + \omega(x)m_2, \tag{31}$$

$$\mu(x)\partial_x m_2 + \mu(\xi)\partial_\xi m_2 = -\mu'(\xi)m_2 - \theta(x)m_1, \tag{32}$$

with boundary conditions

$$m_1(x,x) = \frac{\omega(x)}{\lambda(x)+\mu(x)}, \quad m_2(1,\xi) = 0. \tag{33}$$

The kernel PDEs (31)–(33) is defined over the triangular domain $\mathcal{T} = \{(x,\xi) \mid 0 \le \xi \le x \le 1\}$ and their solution allows to obtain the gain of the observer as:

$$p_1(x) = m_1(x,0)\mu(0), \quad p_2(x) = m_2(x,0)\mu(0). \tag{34}$$

The inverse transformation of (25) is given by

$$\tilde{\beta}(x,t) = \tilde{v}(x,t) + \int_0^x r_2(x,\xi)\tilde{v}(\xi,t)d\xi, \tag{35}$$

where $r_2(x,\xi)$ satisfies

$$r_2(x,\xi) = -m_2(x,\xi) - \int_\xi^x m_2(x,s)r_2(s,\xi)ds. \tag{36}$$

The substitution of (35) into (24) results in

$$\tilde{\alpha}(x,t) = \tilde{u}(x,t) + \int_0^x r_1(x,\xi)\tilde{v}(\xi,t)d\xi, \tag{37}$$

where $r_1(x,\xi) = -m_1(x,\xi) - \int_\xi^x m_1(x,s)r_2(s,\xi)ds$. The invertibility of the transformation (4) together with the existence of a unique solution to (8)–(11) was established in Di Meglio et al. (2013). The exponential stability of the target system governed by (26)–(28) and to that of the error dynamics (21)–(23) is stated in Lemma 3.3 (Di Meglio et al., 2013). The invertibility of the transformation

[1] Here, we use the prime notation to indicate derivatives.

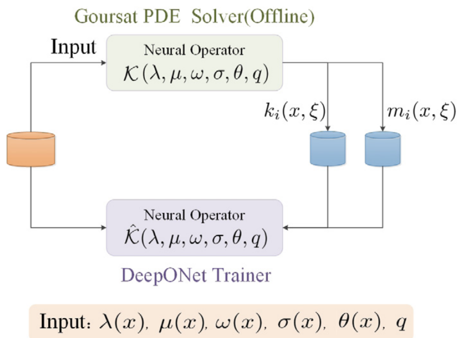

Fig. 1. Learning of the gain kernel functions via DeepONet and through the operator described by the mapping $(\lambda,\mu,\omega,\sigma,\theta,q)\rightarrow(k_1,k_2,m_1,m_2)$. Computing multiple solutions of kernel PDEs (8)–(11) and (31)–(33) in the Goursat form for different functions $\lambda(x)$, $\mu(x)$, $\omega(x)$, $\sigma(x)$, $\theta(x)$ and the parameter q completes the training procedure of the neural operator $\hat{\mathcal{K}}$.

implies the global exponential convergence of the error system in L^2 sense (21)–(23) and the L^2-Global Exponential Stability of the plant (1)–(3) combined with the observer (18)–(20) and subject to the control law

$$U(t)=\int_0^1 k_1(1,\xi)\hat{u}(\xi,t)d\xi+\int_0^1 k_2(1,\xi)\hat{v}(\xi,t)d\xi. \tag{38}$$

We refer the reader to Di Meglio et al. (2013) for more details about the design of the output feedback law (38), turning our attention to the DeepOnet designs for the output feedback law.

Problem statement. As shown in Figs. 1 and 2, we aim at designing neural operators to ultimately learn the controller and observer gain functions governed by (8)–(11) and (31)–(33), respectively. The plant functional coefficients are the inputs of the nonlinear operators defined by these hyperbolic/Goursat PDEs. We first prove a DeepONet approximation to the kernel PDEs by showing the continuity of the mapping from plant coefficients to kernel PDEs solution. The second part of our design consists of the DeepONet encoding of the output-feedback law. Therefore, *proof-based* machine learning designs are presented in this paper.

3. Accuracy of approximation of backstepping kernel operator with DeepONet

As the first step towards defining a DeepOnet approximation of the kernel functions, we recall an important lemma that states the boundedness of the gain kernel functions (Di Meglio et al., 2013).

Lemma 1. *For every $\lambda,\ \mu\in C^1([0,1])$, $\sigma,\ \omega,\ \theta\in C^0([0,1])$, and $q\in\mathbb{R}$, the gain kernels $k_i(x,\xi)$, $m_i(x,\xi)$, $i=1,2$ satisfying the PDE systems (8)–(11) and (31)–(33), respectively, has a unique $C^1(\mathcal{T})$ solution with the following property*

$$|k_i(x,\xi)|\leq N_i e^{M_i},\quad i=1,2,\quad \forall(x,\xi)\in\mathcal{T}, \tag{39}$$

$$|m_i(x,\xi)|\leq N_i e^{M_i},\quad i=1,2,\quad \forall(x,\xi)\in\mathcal{T}, \tag{40}$$

where $N_i>0$, $M_i>0$, $i=1,2$ are constants.

Approximation of the neural operators. Knowing the boundedness of the kernel functions, we introduce two operators that map the functional parameters $\lambda(x)$, $\mu(x)$, $\omega(x)$, $\sigma(x)$, $\theta(x)$ and the constant boundary parameter q of the plant (1)–(3) to the kernel PDEs resulting from the controller and the observer design, namely, (8)–(11) and (31)–(33), respectively. As depicted Fig. 1, we define the neural approximation of the operator $(\lambda,\mu,\omega,\sigma,\theta,q)\mapsto(k_1,\ k_2,\ m_1,\ m_2)$ that consists of the operator $\mathcal{K}:(C^1[0,1])^2\times(C^0[0,1])^3\times\mathbb{R}\mapsto(C^1(\mathcal{T}))^4$, where

$$\begin{aligned}&\mathcal{K}(\lambda,\mu,\sigma,\omega,\theta,q)(x,\xi)\\ &:=(k_1(x,\xi),k_2(x,\xi),m_1(x,\xi),m_2(x,\xi)),\end{aligned} \tag{41}$$

and the operator $\mathcal{M}:(C^1[0,1])^2\times(C^0[0,1])^3\times\mathbb{R}\mapsto(C^1(\mathcal{T}))^2\times(C^0(\mathcal{T}))^4\times(C^0[0,1])^2\times(C^1(\mathcal{T}))^4$ defined as

$$\begin{aligned}&\mathcal{M}(\lambda,\mu,\sigma,\omega,\theta,q)\\ &:=(k_1,k_2,c,\kappa,K_1,K_2,K_3,K_4,K_5,K_6,K_7,K_8),\end{aligned} \tag{42}$$

where

$$K_1(x)=(\lambda(x)+\mu(x))k_1(x,x)+\theta(x), \tag{43}$$

$$K_2(x)=-\lambda(0)qk_1(x,0)+\mu(0)k_2(x,0), \tag{44}$$

$$\begin{aligned}K_3(x,\xi)=&-\mu(x)\partial_x k_1+\lambda(\xi)\partial_\xi k_1+\lambda'(\xi)k_1+\sigma(\xi)k_1\\ &+\theta(\xi)k_2,\end{aligned} \tag{45}$$

$$K_4(x,\xi)=-\mu(x)\partial_x k_2-\mu(\xi)\partial_\xi k_2-\mu'(\xi)k_2+\omega(\xi)k_1, \tag{46}$$

$$\begin{aligned}K_5(x,\xi)=&-\lambda(x)\partial_x m_1+\mu(\xi)\partial_\xi m_1-\mu'(\xi)m_1+\sigma(\xi)m_1\\ &+\omega(x)m_2,\end{aligned} \tag{47}$$

$$K_6(x,\xi)=\mu(x)\partial_x m_2+\mu(\xi)\partial_\xi m_2+\mu'(\xi)m_2+\theta(\xi)m_1, \tag{48}$$

$$K_7(x)=m_1(x,x)(\lambda(x)+\mu(x))-\omega(x), \tag{49}$$

$$K_8(\xi)=m_2(1,\xi), \tag{50}$$

is introduced. The operators $\mathcal{K}$ and $\mathcal{M}$ are useful to state the following theorem.

Theorem 1 (*DeepONet Approximation of the Kernel Functions*)**.** *Consider the neural operator defined in (42), along with (43)–(46) and let $\lambda,\ \mu,\ \sigma,\ \omega,\ \theta,\ \lambda',\ \mu'>0$ be arbitrarily bounded and $\epsilon>0$, there exists a neural operator $\hat{\mathcal{M}}:(C^1[0,1])^2\times(C^0[0,1])^3\times\mathbb{R}\mapsto(C^1(\mathcal{T}))^2\times(C^0(\mathcal{T}))^2\times(C^0[0,1])^2\times(C^1(\mathcal{T}))^4$ such that,*

$$|\mathcal{M}(\lambda,\mu,\sigma,\omega,\theta,q)-\hat{\mathcal{M}}(\lambda,\mu,\sigma,\omega,\theta,q)|<\epsilon, \tag{51}$$

holds for all Lipschitz $\lambda,\ \mu,\ \sigma,\ \omega,\ \theta,\ \lambda',\ \mu'$, namely, there exists a neural operator $\hat{\mathcal{K}}$ such that

$$\begin{aligned}&|\tilde{k}_1|+|\tilde{k}_2|+|\tilde{c}|+|\tilde{\kappa}|+|(\lambda(x)+\mu(x))\tilde{k}_1(x,x)|\\ &+|\lambda(0)q\tilde{k}_1(x,0)-\mu(0)\tilde{k}_2(x,0)|+|-\mu(x)\partial_x\tilde{k}_1\\ &+\lambda(\xi)\partial_\xi\tilde{k}_1+\lambda'(\xi)\tilde{k}_1+\sigma(\xi)\tilde{k}_1+\theta(\xi)\tilde{k}_2|+|-\mu(x)\partial_x\tilde{k}_2\\ &-\mu(\xi)\partial_\xi\tilde{k}_2-\mu'(\xi)\tilde{k}_2+\omega(\xi)\tilde{k}_1|+|\lambda(x)\partial_x\tilde{m}_1-\mu(\xi)\partial_\xi\tilde{m}_1\\ &+\mu'(\xi)\tilde{m}_1-\sigma(\xi)\tilde{m}_1-\omega(x)\tilde{m}_2|+|\mu(x)\partial_x\tilde{m}_2+\mu(\xi)\partial_\xi\tilde{m}_2\\ &+\mu'(\xi)\tilde{m}_2+\theta(\xi)\tilde{m}_1|+|\tilde{m}_1(x,x)(\lambda(x)+\mu(x))|\\ &+|\tilde{m}_2(1,\xi)|<\epsilon,\end{aligned} \tag{52}$$

where $\tilde{c}(x,\xi)=c(x,\xi)-\hat{c}(x,\xi)$, $\tilde{\kappa}(x,\xi)=\kappa(x,\xi)-\hat{\kappa}(x,\xi)$, and

$$\tilde{k}_i(x,\xi)=k_i(x,\xi)-\hat{k}_i(x,\xi),\quad i=1,2, \tag{53}$$

$$\tilde{m}_i(x,\xi)=m_i(x,\xi)-\hat{m}_i(x,\xi),\quad i=1,2, \tag{54}$$

and $(\hat{k}_1(x,\xi),\hat{k}_2(x,\xi),\hat{m}_1(x,\xi),\hat{m}_2(x,\xi))=\hat{\mathcal{K}}(\lambda,\mu,\sigma,\omega,\theta,q)(x,\xi)$.

Proof. The continuity of the operator $\mathcal{M}$ follows from Lemma 1. The result is obtained by invoking (Deng, Shin, Lu, Zhang, & Karniadakis, 2022, Thm. 2.1). ■

4. Output feedback stabilization with DeepONet approximated controller and observer gains

In this section, we prove that the approximated kernel functions where $\hat{k}_i$ and $\hat{m}_i$, $i=1,2$, a priori learned from the DeepOnet layer (offline), enforce the closed-loop system stability

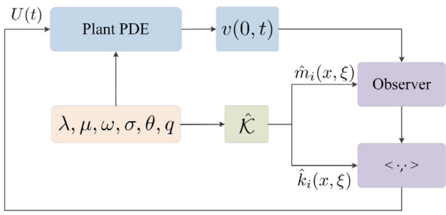

Fig. 2. The PDE backstepping observer (18)–(20) uses boundary measurement of the flux $v(0,t)$. The gains $\hat{k}_i$ and $\hat{m}_i$, $i=1,2$ are produced with the DeepONet $\hat{\mathfrak{K}}$.

with a quantifiable exponential decay rate. The schematic of the resulting closed-loop system is depicted in Fig. 2, consisting of the plant (1)–(3), an observer (18)–(20) together with the output-feedback boundary control law

$$U(t) = \int_0^1 \hat{k}_1(1,\xi)\hat{u}(\xi,t)d\xi + \int_0^1 \hat{k}_2(1,\xi)\hat{v}(\xi,t)d\xi. \tag{55}$$

Applying the certainty equivalence principle, the approximated backstepping transformations (4), (24) and (25) driven by $\hat{k}_i$ and $\hat{m}_i$, $i=1,2$, are defined as

$$\hat{z}(x,t) =\hat{v}(x,t) - \int_0^x \hat{k}_1(x,\xi)\hat{u}(\xi,t)d\xi - \int_0^x \hat{k}_2(x,\xi)\hat{v}(\xi,t)d\xi, \tag{56}$$

$$\tilde{u}(x,t) =\tilde{w}(x,t) + \int_0^x \hat{m}_1(x,\xi)\tilde{z}(\xi,t)d\xi, \tag{57}$$

$$\tilde{v}(x,t) =\tilde{z}(x,t) + \int_0^x \hat{m}_2(x,\xi)\tilde{z}(\xi,t)d\xi. \tag{58}$$

Consequently, the approximation of the neural operator (41) is introduced as

$$(\hat{k}_1(x,\xi), \hat{k}_2(x,\xi), \hat{m}_1(x,\xi), \hat{m}_2(x,\xi)) = \hat{\mathfrak{K}}(\lambda,\mu,\sigma,\omega,\theta,q)(x,\xi). \tag{59}$$

Approximation of the observer system. In light of (56), system (18)–(20) leads to the following approximated target system

$$\begin{aligned}\partial_t\hat{u}(x,t) =& -\lambda(x)\partial_x\hat{u}(x,t) + \sigma(x)\hat{u}(x,t) + \omega(x)\hat{z}(x,t)\\ &+ \int_0^x \hat{c}(x,\xi)\hat{u}(\xi,t)d\xi + \int_0^x \hat{\kappa}(x,\xi)\hat{z}(\xi,t)d\xi\\ &+ \hat{m}_1(x,0)\mu(0)\tilde{z}(0,t),\end{aligned} \tag{60}$$

$$\begin{aligned}\partial_t\hat{z}(x,t) =&\mu(x)\partial_x\hat{z}(x,t) + \delta_1(x)\hat{u}(x,t) + \delta_2(x)\hat{z}(0,t)\\ &+ \int_0^x \delta_3(x,\xi)\hat{u}(\xi,t)d\xi + \int_0^x \delta_4(x,\xi)\hat{v}(\xi,t)d\xi\\ &+ F(x)\mu(0)\tilde{z}(0,t),\end{aligned} \tag{61}$$

$$\hat{u}(0,t) =q\hat{z}(0,t), \quad \hat{z}(1,t) = 0, \tag{62}$$

where

$$\hat{\kappa}(x,\xi) =\omega(x)\hat{k}_2(x,\xi) + \int_\xi^x \hat{\kappa}(x,s)\hat{k}_2(s,\xi)ds, \tag{63}$$

$$\hat{c}(x,\xi) =\omega(x)\hat{k}_1(x,\xi) + \int_\xi^x \hat{c}(x,s)\hat{k}_1(s,\xi)ds, \tag{64}$$

$$\begin{aligned}F(x) =&\hat{m}_2(x,0) - \int_0^x \hat{k}_1(x,\xi)\hat{m}_1(\xi,0)d\xi\\ &- \int_0^x \hat{k}_2(x,\xi)\hat{m}_2(\xi,0)d\xi,\end{aligned} \tag{65}$$

and the approximation error terms, δ_i, $i = 1,2,3,4$ are given below

$$\delta_1(x) =(\lambda(x) + \mu(x))\tilde{k}_1(x,x), \tag{66}$$

$$\delta_2(x) =\lambda(0)q\tilde{k}_1(x,0) - \mu(0)\tilde{k}_2(x,0), \tag{67}$$

$$\begin{aligned}\delta_3(x,\xi) =&\lambda(\xi)'\tilde{k}_1(x,\xi) + \sigma(\xi)\tilde{k}_1(x,\xi) + \theta(\xi)\tilde{k}_2(x,\xi)\\ &- \mu(x)\partial_x\tilde{k}_1(x,y) + \lambda(\xi)\partial_\xi\tilde{k}_1(x,\xi),\end{aligned} \tag{68}$$

$$\begin{aligned}\delta_4(x,\xi) =& - \mu(x)\partial_x\tilde{k}_2(x,y) - \mu(\xi)\partial_\xi\tilde{k}_2(x,\xi)\\ &- \mu(\xi)'\tilde{k}_2(x,\xi) + \omega(\xi)\tilde{k}_1(x,\xi).\end{aligned} \tag{69}$$

Approximation of the observer error system. Similarly, from (57) and (58), system (21)–(23) subject to the approximated kernel functions results into the following PDE system

$$\begin{aligned}\partial_t\tilde{w}(x,t) =& - \lambda(x)\partial_x\tilde{w}(x,t) + \sigma(x)\tilde{w}(x,t)\\ &+ \int_0^x \hat{g}(x,\xi)\tilde{w}(\xi,t)d\xi + \int_0^x \delta_5(x,\xi)\tilde{z}(\xi,t)d\xi\\ &+ \int_0^x\int_\xi^x \hat{r}_1(x,s)\delta_6(s,\xi)ds\tilde{z}(\xi,t)d\xi,\end{aligned} \tag{70}$$

$$\begin{aligned}\partial_t\tilde{z}(x,t) =& \mu(x)\partial_x\tilde{z}(x,t) + \theta(x)\tilde{w}(x,t)\\ &+ \int_0^x \hat{h}(x,\xi)\tilde{w}(\xi,t)d\xi + \int_0^x \delta_6(x,\xi)\tilde{z}(\xi,t)d\xi\\ &+ \int_0^x\int_\xi^x \hat{r}_2(x,s)\delta_6(s,\xi)ds\tilde{z}(\xi,t)d\xi,\end{aligned} \tag{71}$$

$$\tilde{w}(0,t) =0, \quad \tilde{z}(1,t) = 0, \tag{72}$$

where

$$\hat{g}(x,\xi) = -\theta(\xi)\hat{m}_1(x,\xi) - \theta(\xi)\int_\xi^x \hat{m}_1(x,s)\hat{r}_2(s,\xi)ds, \tag{73}$$

$$\hat{h}(x,\xi) = -\theta(\xi)\hat{m}_2(x,\xi) - \theta(\xi)\int_\xi^x \hat{m}_2(x,s)\hat{r}_2(s,\xi)ds. \tag{74}$$

The resulting error terms in the approximated observer error system, δ_i, $i=5,6$, are provided below

$$\begin{aligned}\delta_5(x,\xi) =&\lambda(x)\partial_x\tilde{m}_1(x,\xi) - \mu(\xi)\partial_\xi m_1(x,\xi) - \sigma(x)\tilde{m}_1(x,\xi)\\ &- \omega(x)m_2(x,\xi) + \mu(\xi)'\tilde{m}_1(x,\xi),\end{aligned} \tag{75}$$

$$\begin{aligned}\delta_6(s,\xi) =& - \mu(s)\partial_s\tilde{m}_2(s,\xi) - \mu(\xi)\partial_\xi\tilde{m}_2(s,\xi)\\ &- \mu(\xi)'\tilde{m}_2(s,\xi) - \theta(s)\tilde{m}_1(s,\xi).\end{aligned} \tag{76}$$

Note that from (52), the following inequalities hold

$$\|\delta_i\|_\infty \le \epsilon, \quad i = 1,2,\ldots,6. \tag{77}$$

Next, we state the exponential stability of the approximated target systems (60)–(69) and (70)–(76).

Proposition 1 (*Stability of the Approximated Target System*)**.** *Consider the cascaded target system (60)–(76), there exists $\epsilon^* > 0$ such that for all $\epsilon \in (0,\epsilon^*)$, the following holds*

$$\Psi_1(t) \le \Psi_1(0)\vartheta_2 e^{-\vartheta_1(\epsilon)t}, \quad \forall \ge 0, \tag{78}$$

where ϑ_1, $\vartheta_2 > 0$ and

$$\Psi_1(t) = \|\hat{u}(t)\|^2 + \|\hat{z}(t)\|^2 + \|\tilde{w}(t)\|^2 + \|\tilde{z}(t)\|^2. \tag{79}$$

Proof. The following Lyapunov candidate for the target system (60)–(76)

$$\begin{aligned}V_1(t) =& \int_0^1 \frac{\varrho_1 e^{-\varrho_2 x}}{\lambda(x)}\hat{u}(x,t)^2dx + \int_0^1 \frac{e^{\varrho_2 x}}{\mu(x)}\hat{z}(x,t)^2dx\\ &+ \int_0^1 \frac{\varrho_3 e^{-\varrho_4 x}}{\lambda(x)}\tilde{w}(x,t)^2dx + \int_0^1 \frac{\varrho_5 e^{\varrho_4 x}}{\mu(x)}\tilde{z}(x,t)^2dx,\end{aligned} \tag{80}$$

where $\varrho_i > 0$, $i=1,2,\ldots,5$ are constants to be decided, provides stability at an exponential decay rate to be determined as well. Computing the time derivative of (80) along (60)–(76), and using integration by parts and Young's inequality, the following estimate is obtained[2]:

$$\begin{aligned}\dot V_1(t) \le &-\Bigg(\varrho_1 e^{-\varrho_2}\Bigg(\varrho_2 - \frac{2\bar\sigma+\bar\omega+2\|\hat c\|_\infty+\|\hat\kappa\|_\infty}{\underline\lambda}\\ &-\frac{\bar\mu\|\hat m_1\|_\infty}{\underline\lambda}\Bigg)-\frac{2\epsilon e^{\varrho_2}}{\underline\mu}\Bigg)\|\hat u\|^2-\Bigg(\varrho_2-\frac{\bar\mu\bar F}{\underline\mu}-\frac{4\epsilon e^{\varrho_2}}{\underline\mu}\\ &-\frac{\varrho_1(\bar\omega+\|\hat\kappa\|_\infty)}{\underline\lambda}\Bigg)\|\hat z\|^2-(1-\varrho_1 q^2-\frac{\epsilon e^{\varrho_2}}{\underline\mu})\hat z(0,t)^2\\ &+\frac{\epsilon e^{\varrho_2}}{\underline\mu}\|\hat v\|^2+\Bigg(\frac{\bar\mu\bar F}{\underline\mu}e^{2\varrho_2}+\frac{\varrho_1\bar\mu\|\hat m_1\|_\infty}{\underline\lambda}\Bigg)\tilde z(0,t)^2\\ &-\Bigg(\varrho_3\Bigg(\varrho_4-\frac{2\bar\sigma}{\underline\lambda}-\frac{2\bar\theta\|\hat r_1\|_\infty}{\underline\lambda}\Bigg)e^{-\varrho_4}\\ &-\frac{\varrho_5\bar\theta(1+\|\hat r_2\|_\infty)}{\underline\mu}e^{2\varrho_4}-\frac{\varrho_3\epsilon(1+\|\hat r_1\|_\infty)}{\underline\lambda}\Bigg)\|\tilde w\|^2\\ &-\Bigg(\varrho_5\Bigg(\varrho_4-\frac{\bar\theta(1+\|\hat r_2\|_\infty)}{\underline\mu}\Bigg)-\frac{\varrho_3\epsilon(1+\|\hat r_1\|_\infty)}{\underline\lambda}\\ &-\frac{4\epsilon e^{\varrho_4}}{\underline\mu}\Bigg)\|\tilde z\|^2-\varrho_5\tilde z(0,t)^2, \end{aligned} \tag{81}$$

where $F(x)\le\bar F$ is a bounded function, and $\|\hat c\|_\infty\le\bar\omega\|\hat k_1\|_\infty e^{\|\hat k_1\|_\infty}$, $\|\hat\kappa\|_\infty\le\bar\omega\|\hat k_2\|_\infty e^{\|\hat k_2\|_\infty}$. Since the inverse transformation of the approximated gain kernel (15) allows to derive a bound of the norm of the state $\hat v(x,t)$ in (81) with respect to the norm of the approximated target system's state $\hat u(x,t)$ and $\hat z(x,t)$. In other words,

$$\hat v(x,t)=\hat z(x,t)+\int_0^x \hat l_1(x,\xi)\hat u(\xi,t)d\xi+\int_0^x \hat l_2(x,\xi)\hat z(\xi,t)d\xi, \tag{82}$$

where the inverse kernel $\hat l_i(x,\xi)$ and its inverse $\hat k_i(x,\xi)$, $i=1,2$, satisfy the following equation

$$\hat l_1(x,\xi)=\hat k_1(x,\xi)+\int_\xi^x \hat k_2(x,s)\hat l_1(s,\xi)ds, \tag{83}$$

$$\hat l_2(x,\xi)=\hat k_2(x,\xi)+\int_\xi^x \hat k_2(x,s)\hat l_2(s,\xi)ds, \tag{84}$$

and the following bounds hold

$$\|\hat l_1\|_\infty\le\|\hat k_1\|_\infty e^{\|\hat k_2\|_\infty},\quad \|\hat l_2\|_\infty\le\|\hat k_2\|_\infty e^{\|\hat k_2\|_\infty}. \tag{85}$$

Since $\|k_i-\hat k_i\|_\infty<\epsilon$, using (39), we derive the following bound

$$\|\hat k_i\|_\infty\le N_i e^{M_i}+\epsilon. \tag{86}$$

Substituting (86) into (85) results in the following inequalities

$$\|\hat l_i\|_\infty\le(N_i e^{M_i}+\epsilon)e^{N_2e^{M_2}+\epsilon},\quad i=1,2. \tag{87}$$

Similarly, based on the inverse transformations (35) and (37), we have

$$\tilde w(x,t)=\tilde u(x,t)+\int_0^x \hat r_1(x,\xi)\tilde v(\xi,t)d\xi, \tag{88}$$

$$\tilde z(x,t)=\tilde v(x,t)+\int_0^x \hat r_2(x,\xi)\tilde v(\xi,t)d\xi, \tag{89}$$

where the inverse kernels $\hat r_1(x,\xi)$ and $\hat r_2(x,\xi)$ satisfy equations

$$\hat r_1(x,\xi)=\hat m_1(x,\xi)-\int_\xi^x \hat m_1(x,s)\hat r_2(s,\xi)ds, \tag{90}$$

$$\hat r_2(x,\xi)=-\hat m_2(x,\xi)-\int_\xi^x \hat m_2(x,s)\hat r_2(s,\xi)ds, \tag{91}$$

and the estimates below hold

$$\|\hat r_i\|_\infty\le\|\hat m_i\|_\infty e^{\|\hat m_i\|_\infty},\ i=1,2. \tag{92}$$

Knowing that $\|m_i-\hat m_i\|_\infty<\epsilon$, and using (39), one can deduce that

$$\|\hat m_i\|_\infty\le N_i e^{M_i}+\epsilon. \tag{93}$$

Substituting (93) into (92) gives

$$\|\hat r_i\|_\infty\le(N_i e^{M_i}+\epsilon)e^{N_ie^{M_i}+\epsilon},\quad i=1,2. \tag{94}$$

Based on (82), the following relation holds

$$\|v(t)\|^2\le 3\|\hat l_1\|_\infty^2\|\hat u(t)\|^2+3(1+\|\hat l_2\|_\infty^2)\|\hat z(t)\|^2. \tag{95}$$

Substituting (95) into (81) and selecting the parameters for the Lyapunov function V_1 as (see Wang et al., 2023a for a detailed proof)

$$0<\varrho_1<\min\{\frac{\underline\lambda(\underline\mu\varrho_2-\bar\mu\bar F)}{\underline\mu(\bar\omega+\|\hat\kappa\|_\infty)},\frac{1}{q^2}\}, \tag{96}$$

$$\varrho_2>\max\left\{\frac{2\bar\sigma+\bar\omega+2\|\hat c\|_\infty+\|\hat\kappa\|_\infty+\bar\mu\|\hat m_1\|_\infty}{\underline\lambda},\frac{\bar\mu\bar F}{\underline\mu}\right\}, \tag{97}$$

$$\varrho_3>\frac{\underline\lambda\varrho_5\bar\theta(1+\|\hat r_2\|_\infty)e^{3\varrho_4}}{\underline\mu(\varrho_4\underline\lambda-2(\bar\sigma+\bar\theta\|\hat r_1\|_\infty))}, \tag{98}$$

$$\varrho_4>\max\{\frac{\bar\theta(1+\|\hat r_2\|_\infty)}{\underline\mu},\frac{2\bar\sigma+2\bar\theta\|\hat r_1\|_\infty}{\underline\lambda}\}, \tag{99}$$

$$\varrho_5>\frac{\bar\mu\bar F e^{2\varrho_4}}{\underline\mu}+\frac{\varrho_1\bar\mu\|\hat m_1\|_\infty}{\underline\lambda}, \tag{100}$$

one can define ϵ^* as

$$\begin{aligned}\epsilon^*=\min\Bigg\{&\frac{\underline\mu\varrho_1}{e^{2\varrho_2}(2+3\|\hat l_1\|_\infty^2)}\Bigg(\varrho_2-\frac{2\bar\sigma+2\|\hat c\|_\infty+\|\hat\kappa\|_\infty}{\underline\lambda}\\ &-\frac{\bar\omega+\bar\mu\|\hat m_1\|_\infty}{\underline\lambda}\Bigg),\ \Bigg(\frac{\varrho_2\underline\lambda-\varrho_1(\bar\omega+\|\hat\kappa\|_\infty)}{\underline\lambda}-\frac{\bar\mu\bar F}{\underline\mu}\Bigg)\\ &\cdot\frac{\underline\mu}{e^{\varrho_2}(7+3\|\hat l_2\|_\infty^2)},\ \frac{\varrho_5\underline\lambda(\varrho_4\underline\mu-\bar\theta(1+\|\hat r_2\|_\infty))}{4\underline\lambda e^{\varrho_4}+\underline\mu\varrho_3(1+\|\hat r_1\|_\infty)}\\ &\frac{\underline\lambda}{\varrho_3(1+\|\hat r_1\|_\infty)}\Bigg(\frac{\varrho_3(\varrho_4\underline\lambda-2(\bar\sigma+\bar\theta\|\hat r_1\|_\infty))e^{-\varrho_4}}{\underline\lambda}\\ &-\frac{\varrho_5\bar\theta(1+\|\hat r_2\|_\infty)}{\underline\mu}e^{2\varrho_4}\Bigg),\ \underline\mu(1-\varrho_1q^2)e^{-\varrho_2}\Bigg\}, \end{aligned} \tag{101}$$

such that for all $\epsilon\in(0,\epsilon^*)$, $\dot V_1(t)\le-\vartheta_1(\epsilon)V_1(t)$, where $\vartheta_1(\epsilon)$ is defined by

$$\begin{aligned}\vartheta_1(\epsilon)=\min\Bigg\{&\frac{\underline\lambda}{\varrho_1}\Bigg(\varrho_1e^{-\varrho_2}\Bigg(\varrho_2-\frac{2\bar\sigma+\bar\omega+2\|\hat c\|_\infty+\|\hat\kappa\|_\infty}{\underline\lambda}\\ &-\frac{\bar\mu\|\hat m_1\|_\infty}{\underline\lambda}\Bigg)-\frac{\epsilon e^{\varrho_2}(2+3\|\hat l_1\|_\infty^2)}{\underline\mu}\Bigg),\ \frac{\underline\mu}{e^{\varrho_2}}\Bigg(\varrho_2\\ &-\frac{\varrho_1(\bar\omega+\|\hat\kappa\|_\infty)}{\underline\lambda}-\frac{\bar\mu\bar F}{\underline\mu}-\frac{7\epsilon e^{\varrho_2}}{\underline\mu}-\frac{3\epsilon e^{\varrho_2}\|\hat l_2\|_\infty^2}{\underline\mu}\Bigg),\\ &\frac{\underline\lambda e^{-\varrho_4}}{\varrho_3}\Bigg(\varrho_3\Bigg(\varrho_4-\frac{2\bar\sigma}{\underline\lambda}-\frac{2\bar\theta\|\hat r_1\|_\infty}{\underline\lambda}\Bigg)-\frac{\varrho_3\epsilon(1+\|\hat r_1\|_\infty)}{\underline\lambda}\\ &-\frac{\varrho_5\bar\theta(1+\|\hat r_2\|_\infty)}{\underline\mu}e^{2\varrho_4}\Bigg),\ \frac{\underline\mu}{\varrho_5e^{\varrho_4}}\Bigg(\varrho_5\Bigg(\varrho_4-\frac{\bar\theta\|\hat r_2\|_\infty}{\underline\mu}\\ &-\frac{\bar\theta}{\underline\mu}\Bigg)-\frac{\varrho_3\epsilon(1+\|\hat r_1\|_\infty)}{\underline\lambda}-\frac{4\epsilon e^{\varrho_4}}{\underline\mu}\Bigg)\Bigg\}, \end{aligned} \tag{102}$$

[2] Due to page limits, complete proofs are in the unabridged manuscript (Wang, Diagne, & Krstic, 2023a).

which leads that $V_1(t) \le V_1(0)e^{-\vartheta_1(\epsilon)t}$. From (79), we have

$$V_1(t) \le \max\left\{\frac{\varrho_1}{\underline{\lambda}}, \frac{\varrho_3}{\underline{\lambda}}, \frac{e^{\varrho_2}}{\underline{\mu}}, \frac{\varrho_5 e^{\varrho_4}}{\underline{\mu}}\right\}\Psi_1(t), \tag{103}$$

$$\Psi_1(t) \le \frac{1}{\min\left\{\frac{\varrho_1 e^{-\varrho_2}}{\bar{\lambda}}, \frac{\varrho_3 e^{-\varrho_4}}{\bar{\lambda}}, \frac{1}{\bar{\mu}}, \frac{\varrho_5}{\bar{\mu}}\right\}} V_1(t). \tag{104}$$

Therefore, the exponential stability bound (78) holds, and

$$\begin{aligned}\vartheta_2 = &\min\left\{\frac{\varrho_1 e^{-\varrho_2}}{\bar{\lambda}}, \frac{\varrho_3 e^{-\varrho_4}}{\bar{\lambda}}, \frac{1}{\bar{\mu}}, \frac{\varrho_5}{\bar{\mu}}\right\} \\ &\cdot \max\left\{\frac{\varrho_1}{\underline{\lambda}}, \frac{\varrho_3}{\underline{\lambda}}, \frac{e^{\varrho_2}}{\underline{\mu}}, \frac{\varrho_5 e^{\varrho_4}}{\underline{\mu}}\right\}. \quad \blacksquare\end{aligned} \tag{105}$$

The following proposition states the stability equivalence between the target system and the original closed-loop system. Transformations (56), (58), along with their inverse (82), (88) and (89) help to state the following norm-equivalence properties.

Proposition 2 (*Norm Equivalence Between Approximated Target and Original Systems*). *Consider the closed-loop system including the plant (1)–(3) with observer system (18)–(20) and the observer-based controller (55). There exists $\epsilon^* > 0$ such that for all $\epsilon \in (0, \epsilon^*)$, the following estimates hold between this closed-loop system and the target system (60)–(76),*

$$\Psi_1(t) \le S_1(\epsilon)\Phi_1(t), \quad \Phi_1(t) \le S_2(\epsilon)\Psi_1(t), \tag{106}$$

where

$$\Phi_1(t) = \|u(t)\|^2 + \|v(t)\|^2 + \|\hat{u}(t)\|^2 + \|\hat{v}(t)\|^2, \tag{107}$$

$\Psi_1(t)$ is defined in (79) and the positive constants as

$$\begin{aligned}S_1(\epsilon) =& 20 + 8(N_1 e^{M_1} + \epsilon)e^{N_1 e^{M_1}+\epsilon} + 8(N_2 e^{M_2} + \epsilon) \\ &\cdot e^{N_2 e^{M_2}+\epsilon} + 3(N_1 e^{M_1} + N_2 e^{M_2} + 2\epsilon),\end{aligned} \tag{108}$$

$$\begin{aligned}S_2(\epsilon) =& 20 + 9(N_1 e^{M_1} + N_2 e^{M_2} + 2\epsilon)\, e^{N_2 e^{M_2}+\epsilon} + 4N_1 e^{M_1} \\ &+ 4N_2 e^{M_2} + 8\epsilon.\end{aligned} \tag{109}$$

Proof. From (56)–(58), we have[3]

$$\begin{aligned}\Psi_1(t) =& \|\hat{u}(t)\|^2 + \int_0^1 \left(\hat{v}(x,t) - \int_0^x \hat{k}_1(x,\xi)\hat{u}(\xi,t)d\xi \right. \\ &\left. - \int_0^x \hat{k}_2(x,\xi)\hat{v}(\xi,t)d\xi\right)^2 dx \\ &+ \int_0^1 \left(\tilde{u}(x,t) + \int_0^x \hat{r}_1(x,\xi)\tilde{v}(\xi,t)d\xi\right)^2 dx \\ &+ \int_0^1 \left(\tilde{v}(x,t) + \int_0^x \hat{r}_2(x,\xi)\tilde{v}(\xi,t)d\xi\right)^2 dx \\ \le& (1 + 3\|\hat{k}_1\|_\infty^2)\|\hat{u}(t)\|^2 + 3(1 + \|\hat{k}_2\|_\infty^2)\|\hat{v}(t)\|^2 \\ &+ 2\|\tilde{u}(t)\|^2 + 2(1 + \|\hat{r}_1\|_\infty^2 + \|\hat{r}_2\|_\infty^2)\|\tilde{v}(t)\|^2.\end{aligned} \tag{110}$$

Since $\tilde{u} = u - \hat{u}$ and $\tilde{v} = v - \hat{v}$, we have

$$\begin{aligned}\Psi_1(t) \le& (1 + 3\|\hat{k}_1\|_\infty^2)\|\hat{u}(t)\|^2 + 3(1 + \|\hat{k}_2\|_\infty^2)\|\hat{v}(t)\|^2 \\ &+ 2\|u(t) - \hat{u}(t)\|^2 + 2(1 + \|\hat{r}_1\|_\infty^2 + \|\hat{r}_2\|_\infty^2) \\ &\cdot \|v(t) - \hat{v}(t)\|^2 \\ \le& (20 + 3\|\hat{k}_1\|_\infty^2 + 3\|\hat{k}_2\|_\infty^2 + 8\|\hat{r}_1\|_\infty^2 + 8\|\hat{r}_2\|_\infty^2)\Phi_1(t).\end{aligned} \tag{111}$$

Submiting (86) and (94) into (111), it arrivals

$$\begin{aligned}\Psi_1(t) \le& \Big(20 + 8(N_1 e^{M_1} + \epsilon)e^{N_1 e^{M_1}+\epsilon} + 8(N_2 e^{M_2} + \epsilon) \\ &\cdot e^{N_2 e^{M_2}+\epsilon} + 3(N_1 e^{M_1} + N_2 e^{M_2} + 2\epsilon)\Big)\, \Phi_1(t).\end{aligned} \tag{112}$$

Similarly, from (57), (58), and (82), we obtain

$$\begin{aligned}\Phi_1(t) \le& (3 + 9\|\hat{l}_1\|_\infty^2)\|\hat{u}(t)\|^2 + 9(1 + \|\hat{l}_2\|_\infty^2)\|\hat{z}(t)\|^2 \\ &+ 4\|\tilde{w}(t)\|^2 + 4(1 + \|\hat{m}_1\|_\infty^2 + \|\hat{m}_2\|_\infty^2)\|\tilde{z}(t)\|^2 \\ \le& (20 + 9(N_1 e^{M_1} + N_2 e^{M_2} + 2\epsilon)\, e^{N_2 e^{M_2}+\epsilon} \\ &+ 4N_1 e^{M_1} + 4N_2 e^{M_2} + 8\epsilon)\Psi_1(t),\end{aligned} \tag{113}$$

which completes the proof. $\blacksquare$

After establishing the norm-equivalence in Proposition 2, the main result immediately follows in Theorem 2.

Theorem 2 (*Main Result—Exponential Stabilization via DeepONet Controller and Observer Gains*). *Consider the closed-loop system consisting of the plant (1)–(3) together with the observer (18)–(20) and the control law (55). Assuming that functions $\lambda, \mu \in C^1([0,1])$ have Lipschitz derivatives, $\sigma, \omega, \theta \in C^0([0,1])$, $q \in \mathbb{R}$, and let $\lambda, \mu, \sigma, \omega, \theta, \lambda', \mu' > 0$ be arbitrarily bounded, there exists a sufficiently small $\epsilon^* > 0$ such that all gain in the feedback law (55) and the observer system (18)–(20) with the neural operator $\hat{\mathcal{M}}(\lambda, \mu, \sigma, \omega, \theta, q)$ of approximation accuracy $\epsilon \in (0, \epsilon^*)$ in relation to the exact backstepping kernels $k_i(x,\xi)$, and $m_i(x,\xi)$, $i = 1, 2$ that ensures the following exponential stability bound*

$$\Phi_1(t) \le \Phi_1(0)S_1(\epsilon)S_2(\epsilon)\vartheta_2 e^{-\vartheta_1(\epsilon)t}, \quad \forall t \ge 0, \tag{114}$$

where $\vartheta_1, \vartheta_2 > 0$ are positive constants, $\Phi_1(t)$, $S_1(\epsilon)$ and $S_2(\epsilon)$ are defined in (107)–(109), respectively.

Remark 1. The product $S_1(\epsilon)S_2(\epsilon)$ is the portion of the overshoot which depends on ϵ and this dependence is clearly increasing, based on (108) and (109). It makes sense that poor approximation increases the overshoot estimate. The definition of the decay rate ϑ_1, as given (102), shows a decreasing dependence on ϵ, meaning that a poor approximation reduces the decay rate estimate.

5. A fully learned output feedback law via DeepONet approximation

5.1. Summary of the design procedure

In this section, we present a DeepONet approximation design that enables one to achieve learning of the output-feedback boundary control signal and provide proof-equipped stability guarantees. Exploiting the kernel functions approximation obtained in Section 4, we design a DeepONet that take as entries the five plant parameters $\lambda(x)$, $\mu(x)$, $\sigma(x)$, $\omega(x)$, $\theta(x)$ and q, as well as the estimates generated by the state observer, namely, $\hat{u}(x,t)$, $\hat{v}(x,t)$. The learning network is built to produce the following approximated control law

$$\hat{U}(t) = \int_0^1 \hat{k}_1(1,\xi)\hat{u}(\xi,t)d\xi + \int_0^1 \hat{k}_2(1,\xi)\hat{v}(\xi,t)d\xi. \tag{115}$$

The structure of the DeepONet-assisted closed-loop system is depicted in Fig. 3. Our result only ensures semi-global practical exponential stability (SG-PES) because as opposed to the approach presented in Section 4, which only contains multiplicative error, the mapping $\hat{U}(t)$ in (115), involves an additive intermediate linear layer that supplements additive error into the approximation process. We proceed with the three following steps (see Fig. 3):

[3] Due to page limits, complete proofs are in the unabridged manuscript (Wang et al., 2023a).

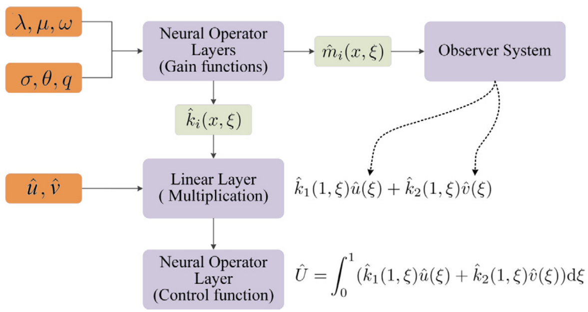

Fig. 3. The learning architecture of the observer-based control law in three steps.

- **Step 1.** The functions $\lambda(x)$, $\mu(x)$, $\sigma(x)$, $\omega(x)$, $\theta(x)$, q remain the inputs of the neural operator $\mathcal{K}$ introduced in Section 4 and generates the NO approximated kernel functions $\hat{k}_i(x,\xi)$ and $\hat{m}_i(x,\xi)$, $i = 1, 2$.
- **Step 2.** A linear layer is employed to multiply the estimated kernel functions $\hat{k}_i(x,\xi)$, $i = 1, 2$ with the observer estimates $\hat{u}$ and $\hat{v}$.
- **Step 3.** A new neural operator $\mathcal{U} : (\lambda, \mu, \sigma, \omega, \theta, q, \hat{u}, \hat{v}) \mapsto U$, $(C^1[0,1])^2 \times (C^0[0,1])^3 \times \mathbb{R} \times (C^0[0,1])^2 \mapsto \mathbb{R}$, where U is defined in (38), is learned to implement the nonlinear integral operation, resulting in the final observer-based control law $\hat{U}$ given by (115). This mapping is constructed using the DeepONet approximation accuracy theorem recently introduced in Krstic et al. (2024) for a reaction–diffusion PDE.

The expansion of the mapping $\mathcal{K}$ defined in **Step 1** from larger space $\mathcal{U}$ to the scalar value of the control input $\hat{U}(t)$ comes at the price of a substantial amount of training and learning effort.

Let us denote $\hat{\mathcal{U}}$ the NO approximation of the output-feedback operator $\mathcal{U}$ and recall the operator $\hat{\mathcal{M}}$ given in Theorem 1, the following theorem holds.

Theorem 3 (*DeepONet Approximation of the Output Feedback Control Law*)**.** *Let λ, μ, σ, ω, θ, λ', $\mu' > 0$ be arbitrarily bounded and $\epsilon > 0$, there exists neural operators $\hat{\mathcal{M}}$ and $\hat{\mathcal{U}}$ such that*

$$\begin{aligned}&|\mathcal{M}(\lambda,\mu,\sigma,\omega,\theta,q)(x,\xi) - \hat{\mathcal{M}}(\lambda,\mu,\sigma,\omega,\theta,q)(x,\xi)| \\ &+ |\mathcal{U}(\lambda,\mu,\sigma,\omega,\theta,q,\hat{u},\hat{v}) - \hat{\mathcal{U}}(\lambda,\mu,\sigma,\omega,\theta,q,\hat{u},\hat{v})| < \epsilon, \quad (116)\end{aligned}$$

holds for all Lipschitz λ, μ, σ, ω, θ, λ', μ', $\hat{u}$, $\hat{v}$ with the properties that $\|\hat{u}(t)\|_\infty \le B_{\hat{u}}$, $\|\hat{v}(t)\|_\infty \le B_{\hat{v}}$, namely, there exists a neural operator $\hat{\mathcal{K}}$ such that

$$\begin{aligned}&|\tilde{k}_1| + |\tilde{k}_2| + |\tilde{c}| + |\tilde{\kappa}| + |(\lambda(x) + \mu(x))\tilde{k}_1(x,x)| \\ &+ |\lambda(0)q\tilde{k}_1(x,0) - \mu(0)\tilde{k}_2(x,0)| + |\lambda(\xi)\partial_\xi \tilde{k}_1 - \mu(x)\partial_x \tilde{k}_1 \\ &+ \lambda'(\xi)\tilde{k}_1 + \sigma(\xi)\tilde{k}_1 + \theta(\xi)\tilde{k}_2| + | - \mu(x)\partial_x \tilde{k}_2 - \mu(\xi)\partial_\xi \tilde{k}_2 \\ &- \mu'(\xi)\tilde{k}_2 + \omega(\xi)\tilde{k}_1| + |\lambda(x)\partial_x \tilde{m}_1 - \mu(\xi)\partial_\xi \tilde{m}_1 + \mu'(\xi)\tilde{m}_1 \\ &-\sigma(\xi)\tilde{m}_1 - \omega(x)\tilde{m}_2| + |\mu(x)\partial_x \tilde{m}_2 + \mu(\xi)\partial_\xi \tilde{m}_2 + \mu'(\xi)\tilde{m}_2 \\ &+\theta(\xi)\tilde{m}_1| + |\tilde{\mathcal{U}}(\lambda,\mu,\sigma,\omega,\theta,q,\hat{u},\hat{v})| < \epsilon. \quad (117)\end{aligned}$$

Proof. The continuity of the operator $\mathcal{M}$ follows directly from Lemma 1 and that of the operator $\mathcal{U}$ can be established following (Bhan et al., 2024b, Lem. 4). The final result is then obtained by invoking (Deng et al., 2022, Thm. 2.1). ■

Theorem 3 is useful to prove the stability of (1)–(3) combined with the observer system (18)–(20) when the approximated output feedback control law (115) learned through DeepOnet is assigned.

5.2. Stabilization under output feedback control law generated via DeepONet

Recalling the NO approximation $\hat{\mathcal{U}}$, the control law (115) can be expressed as $\hat{U} = \hat{\mathcal{U}}(\lambda,\mu,\sigma,\omega,\theta,q,\hat{u},\hat{v})$. Applying the certainty equivalence principle, the backstepping transformations (4), (24) and (25) driven by $\hat{k}_i$ and $\hat{m}_i$, $i = 1, 2$, are defined as (56)–(58), respectively. The inverse transformations of (56)–(58) are defined in (82), (88) and (89), respectively.

Using the backstepping transformation (56), the observer (18)–(20) translates into the following target system

$$\begin{aligned}\partial_t \hat{u}(x,t) = &- \lambda(x)\partial_x \hat{u}(x,t) + \sigma(x)\hat{u}(x,t) + \omega(x)\hat{z}(x,t) \\ &+ \int_0^x \hat{c}(x,\xi)\hat{u}(\xi,t)d\xi + \int_0^x \hat{\kappa}(x,\xi)\hat{z}(\xi,t)d\xi \\ &+ \hat{m}_1(x,0)\mu(0)\tilde{z}(0,t), \quad (118)\end{aligned}$$

$$\partial_t \hat{z}(x,t) = \mu(x)\partial_x \hat{z}(x,t) + F(x)\mu(0)\tilde{z}(0,t), \quad (119)$$

$$\hat{u}(0,t) = q\hat{z}(0,t), \quad \hat{z}(1,t) = \tilde{U}(t), \quad (120)$$

where $\hat{\kappa}(x,\xi)$, $\hat{c}(x,\xi)$ and $F(x)$ are defined in (63)–(65), respectively. The approximation error terms, δ_i, $i = 1, 2, 3, 4$ are given in (66)–(69), and $\tilde{U}(t) = U(t) - \hat{U}(t)$. We recall that $U(t)$, the approximated control law (115), is obtained from an approximation of the gain kernel when functions parameters $\lambda(x)$, $\mu(x)$, $\sigma(x)$, $\omega(x)$, $\theta(x)$ vary whereas, the complete approximation of the feedback law, namely, $\hat{U}(t)$, requires input–output data of the observer states, namely, $\hat{u}$ and $\hat{v}$, provided some L^2 initial data $(u_0(x), v_0(x), \hat{u}_0(x), \hat{v}_0(x))$. It is worth recalling that the estimated state trajectories result from a dataset collected at the sensing point $v(0,t)$.

Using (57) and (58), the error system (21)–(23) maps into the following set of PDEs

$$\begin{aligned}\partial_t \tilde{w}(x,t) = &- \lambda(x)\partial_x \tilde{w}(x,t) + \sigma(x)\tilde{w}(x,t) \\ &+ \int_0^x \hat{g}(x,\xi)\tilde{w}(\xi,t)\mathrm{d}\xi + \int_0^x \delta_5(x,\xi)\tilde{z}(\xi,t)\mathrm{d}\xi \\ &+ \int_0^x \int_\xi^x \hat{r}_1(x,s)\delta_6(s,\xi)\mathrm{d}s\tilde{z}(\xi,t)\mathrm{d}\xi, \quad (121)\end{aligned}$$

$$\begin{aligned}\partial_t \tilde{z}(x,t) = &\mu(x)\partial_x \tilde{z}(x,t) + \theta(x)\tilde{w}(x,t) \\ &+ \int_0^x \hat{h}(x,\xi)\tilde{w}(\xi,t)\mathrm{d}\xi + \int_0^x \delta_6(x,\xi)\tilde{z}(\xi,t)\mathrm{d}\xi \\ &+ \int_0^x \int_\xi^x \hat{r}_2(x,s)\delta_6(s,\xi)\mathrm{d}s\tilde{z}(\xi,t)\mathrm{d}\xi, \quad (122)\end{aligned}$$

$$\tilde{w}(0,t) = 0, \quad \tilde{z}(1,t) = \tilde{U}(t), \quad (123)$$

where $\hat{g}(x,\xi)$, $\hat{h}(x,\xi)$, $\delta_5(x,\xi)$ and $\delta_6(x,\xi)$ are defined in (73)–(76), respectively.

We claim that the coupled target system (118)–(120), (121)–(123), equipped with the DeepONet-based approximated kernels, is semi-globally practically exponentially stable.

Proposition 3 (*Stability of the Approximated Target System*)**.** *Consider the cascaded target system (118)–(120), (121)–(123), there exists $\varepsilon^* > 0$ such that for all $\varepsilon \in (0, \varepsilon^*)$, and the following holds*

$$\Psi_2(t) \le \Psi_2(0)\vartheta_4(\epsilon)\mathrm{e}^{-\vartheta_3(\epsilon)t} + \vartheta_5\epsilon^2, \quad \forall t \ge 0, \quad (124)$$

where $\Psi_2(t) = \|\hat{u}(t)\|^2 + \|\hat{z}(t)\|^2 + \|\tilde{w}(t)\|^2 + \|\tilde{z}(t)\|^2$, and

$$\begin{aligned}\vartheta_3(\epsilon) = \min\Bigg\{&\underline{\lambda} e^{-\iota_2}\left(\iota_2 - \frac{2\bar{\sigma} + \bar{\omega} + 2\|\hat{c}\|_\infty + \|\hat{\kappa}\|_\infty}{\underline{\lambda}} \right. \\ &\left. - \frac{\bar{\mu}\|\hat{m}_1\|_\infty}{\underline{\lambda}}\right), \frac{\underline{\mu}}{e^{\iota_2}}\left(\iota_2 - \frac{\iota_1(\bar{\omega} + \|\hat{\kappa}\|_\infty)}{\underline{\lambda}} - \frac{\bar{\mu}\bar{F}}{\underline{\mu}}\right),\end{aligned}$$

$$\frac{\underline{\lambda}e^{-\iota_4}}{\iota_3}\Bigg(\iota_3\Bigg(\iota_4-\frac{2\bar{\sigma}}{\underline{\lambda}}-\frac{2\bar{\theta}\|\hat{r}_1\|_\infty}{\underline{\lambda}}\Bigg)-\frac{\iota_3\epsilon(1+\|\hat{r}_1\|_\infty)}{\underline{\lambda}}-\frac{\iota_5\bar{\theta}(1+\|\hat{r}_2\|_\infty)}{\underline{\mu}}e^{2\iota_4}\Bigg),\ \frac{\underline{\mu}}{\iota_5 e^{\iota_4}}\Bigg(\iota_5\Bigg(\iota_4-\frac{\bar{\theta}(1+\|\hat{r}_2\|_\infty)}{\underline{\mu}}\Bigg)-\frac{4\epsilon e^{\iota_4}}{\underline{\mu}}-\frac{\iota_3\epsilon(1+\|\hat{r}_1\|_\infty)}{\underline{\lambda}}\Bigg)\Bigg\},\quad \vartheta_4(\epsilon)=\frac{e^{\iota_2}+\iota_5 e^{\iota_4}}{\vartheta_3(\epsilon)}, \tag{125}$$

$$\vartheta_5=\min\left\{\frac{\iota_1 e^{-\iota_2}}{\bar{\lambda}},\ \frac{\iota_3 e^{-\iota_4}}{\bar{\lambda}},\ \frac{1}{\bar{\mu}},\ \frac{\iota_5}{\bar{\mu}}\right\}\cdot\max\left\{\frac{\iota_1}{\underline{\lambda}},\ \frac{\iota_3}{\underline{\lambda}},\ \frac{e^{\iota_2}}{\underline{\mu}},\ \frac{\iota_5 e^{\iota_4}}{\underline{\mu}}\right\}, \tag{126}$$

with $0<\iota_1<\frac{1}{q^2}$,

$$\iota_2>\max\left\{\frac{2\bar{\sigma}+\bar{\omega}+2\|\hat{c}\|_\infty+\|\hat{\kappa}\|_\infty+\bar{\mu}\|\hat{m}_1\|_\infty}{\underline{\lambda}},\ \frac{\iota_1(\bar{\omega}+\|\hat{\kappa}\|_\infty)}{\underline{\lambda}}+\frac{\bar{\mu}\bar{F}}{\underline{\mu}}\right\}, \tag{127}$$

$$\iota_3>\frac{\underline{\lambda}\iota_5\bar{\theta}(1+\|\hat{r}_2\|_\infty)e^{3\iota_4}}{\underline{\mu}(\iota_4\underline{\lambda}-2(\bar{\sigma}+\bar{\theta}\|\hat{r}_1\|_\infty))}, \tag{128}$$

$$\iota_4>\max\{\frac{\bar{\theta}(1+\|\hat{r}_2\|_\infty)}{\underline{\mu}},\ \frac{2\bar{\sigma}+2\bar{\theta}\|\hat{r}_1\|_\infty}{\underline{\lambda}}\}, \tag{129}$$

$$\iota_5>\frac{\bar{\mu}\bar{F}e^{2\iota_2}}{\underline{\mu}}+\frac{\iota_1\bar{\mu}\|\hat{m}_1\|_\infty}{\underline{\lambda}}. \tag{130}$$

Moreover, we define ϵ^* *as*

$$\epsilon^*=\min\left\{\frac{\underline{\lambda}}{\iota_1(1+\|\hat{r}_1\|_\infty)}\left(\frac{\iota_3(\iota_4\underline{\lambda}-2(\bar{\sigma}+\bar{\theta}\|\hat{r}_1\|_\infty))e^{-\iota_4}}{\underline{\lambda}}-\frac{\iota_5\bar{\theta}(1+\|\hat{r}_2\|_\infty)}{\underline{\mu}}e^{2\iota_4}\right),\ \frac{\iota_5\underline{\lambda}(\iota_4\underline{\mu}-\bar{\theta}(1+\|\hat{r}_2\|_\infty))}{4\underline{\lambda}e^{\iota_2}+\underline{\mu}\iota_3(1+\|\hat{r}_1\|_\infty)}\right\}. \tag{131}$$

The proof of Proposition 3 is given in Wang et al. (2023a).

To translate the stability of the cascaded target system into that of the original closed-loop system, we consider transformations (56)–(58), along with inverse transformations (82), (88) and (89), and state the following proposition.

Proposition 4 (*Norm Equivalence Between Approximated Target and Original Systems*)**.** *Consider the closed-loop system including the plant (1)–(3) with observer system (18)–(20) and the observer-based controller (115). There exists* $\epsilon^*>0$ *such that for all* $\epsilon\in(0,\epsilon^*)$*, the following estimates hold between this closed-loop system and the cascaded target system (118)–(120), (121)–(123),* $\Psi_2(t)\le S_1(\epsilon)\Phi_2(t)$*,* $\Phi_2(t)\le S_2(\epsilon)\Psi_2(t)$*, where* $\Phi_2(t)=\|u(t)\|^2+\|v(t)\|^2+\|\hat{u}(t)\|^2+\|\hat{v}(t)\|^2$*, and the positive constants are given in (108) and (109), respectively.*

The proof of Proposition 4 is similar to that of Proposition 2 and can be found in Wang et al. (2023a). With the help of Propositions 3 and 4 state we state following theorem.

Theorem 4 (*Semi-global Practical Exponential Stability via DeepOnet Controller and Observer Gains*)**.** *For any* $\epsilon<\epsilon^*$ *where*

$$\epsilon^*:=\frac{\sqrt{(B_u^2+B_v^2+B_{\hat{u}}^2+B_{\hat{v}}^2)}}{\sqrt{S_2(\epsilon)\vartheta_5}}>0, \tag{132}$$

and $\|u(0)\|^2+\|v(0)\|^2+\|\hat{u}(0)\|^2+\|\hat{v}(0)\|^2\le\zeta$*, where*

$$\zeta:=\frac{S_1(\epsilon)}{S_2(\epsilon)\vartheta_4(\epsilon)}\left((B_u^2+B_v^2+B_{\hat{u}}^2+B_{\hat{v}}^2)-S_2(\epsilon)\vartheta_5\epsilon^2\right)>0, \tag{133}$$

the closed-loop system consisting of the NO approximation of the PDE feedback law (115) and the plant (1)–(3) and observer system (18)–(20) satisfy the semi-global practical exponential stability estimate,

$$\Phi_2(t)\le\frac{S_2(\epsilon)}{S_1(\epsilon)}\vartheta_4(\epsilon)e^{-\vartheta_3(\epsilon)t}\Phi_2(0)+S_2\vartheta_5\epsilon^2,\quad\forall t\ge 0. \tag{134}$$

Remark 2. The estimate given by (134) is semi-global, allowing the radius ζ of the initial condition ball in the $L^2[0,1]$ space to expand as B_u, B_v, $B_{\hat{u}}$, and $B_{\hat{v}}$ increase. Additionally, the size of the training set and the number of neural network nodes are functions of these parameters. Despite the semi-global stability, the region of attraction ζ, defined in (133), is much smaller than the magnitude of samples associated with B_u, B_v, $B_{\hat{u}}$, and $B_{\hat{v}}$ in the training set. From (134), as $t\to\infty$, the residual value $\Phi_2(t)\le S_2\vartheta_5\epsilon^2$ can be minimized by decreasing ϵ and simultaneously increasing the training set size and the number of neural network nodes accordingly.

6. Simulation results

Our simulation[4] is performed considering a 2×2 linear hyperbolic system with $\lambda(x)=\Gamma x+1$, $\mu(x)=e^{\Gamma x}+2$, $\delta(x)=\Gamma(x+1)$, $\theta(x)=\Gamma(x+1)$, $\omega(x)=\Gamma(\cosh(x)+1)$, $q=\Gamma/3$, parameterized by $\Gamma=5$. Under initial conditions $u_0(x)=1$, $v_0(x)=\sin(x)$. By iterating the functions $\lambda(x)$, $\mu(x)$, $\delta(x)$, $\theta(x)$, and $\omega(x)$ along the y-axis to generate a two-dimensional (2D) input for the $\mathcal{K}$ network, the DeepONet is developed without modifying the grid structure. Similarly, the constant q is iterated along both x and y coordinates to generate additional 2D inputs for the $\mathcal{K}$ network. In summary, this methodology results in six distinct 2D inputs for the network. Our approach capitalizes on this 2D structure by integrating a Convolutional Neural Network (CNN) into the branch network of the DeepONet. Exploiting a 2000 samples dataset, the model demonstrating the highest accuracy in data point classification is identified. The error between analytical and learned DeepONet kernels, namely k_1, k_2, m_1, and m_2, are depicted in Figs. 4. These figures illustrate the kernels' behavior for the value of $\Gamma=5$. During the training phase, the relative L^2 errors for kernels k_1, k_2, m_1, and m_2 were recorded as 4.90×10^{-5}, 3.48×10^{-5}, 6.69×10^{-5}, and 2.61×10^{-5}, respectively. The corresponding testing errors were 5.32×10^{-5}, 3.89×10^{-5}, 7.34×10^{-5}, and 2.62×10^{-5}.

Furthermore, we simulate the closed-loop system comprising the NO approximation of the PDE feedback law (115), the plant (1)–(3), and the observer system (18)–(20). Our control law is derived using a pre-designed learning network for the gain kernels, rather than directly from the inputs $\lambda(x)$, $\mu(x)$, $\sigma(x)$, $\omega(x)$, $\theta(x)$, q, $\hat{u}(x,t)$, and $\hat{v}(x,t)$. These inputs are processed by the neural operators from Section 4 to approximate kernel functions $\hat{k}_i(x,\xi)$ and $\hat{m}_i(x,\xi)$, $i=1,2$. These approximations are then linearly combined with observer estimates $\hat{u}$ and $\hat{v}$. Finally, using a DeepONet layer to learn the mapping $(\lambda,\mu,\sigma,\omega,\theta,q,\hat{u},\hat{v})\to\hat{U}$ from 2000 samples, we achieve a convergence error of 5.46×10^{-8} in L^2 and a testing error of 5.97×10^{-8}. Fig. 5 illustrates the feasibility of both control laws $U(t)$ and $\hat{U}(t)$.

[4] We refer the reader to Wang et al. (2023a) where expanded simulation results including the training loss, the convergence of the observer and the error system can be found.

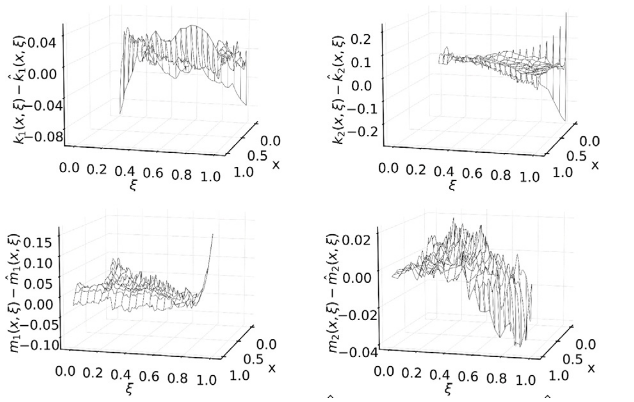

Fig. 4. The error between approximated and exact gain kernel functions $k_1(x,\xi)-\hat{k}_1(x,\xi)$, $k_2(x,\xi)-\hat{k}_2(x,\xi)$, $m_1(x,\xi)-\hat{m}_1(x,\xi)$ and $m_2(x,\xi)-\hat{m}_2(x,\xi)$.

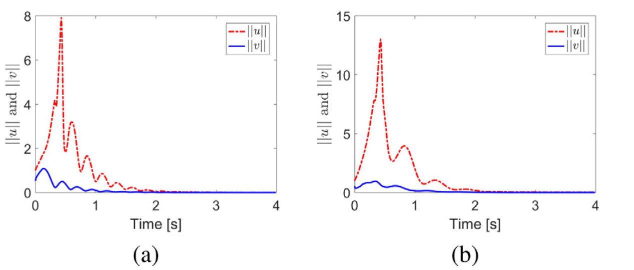

Fig. 5. (a): The closed-loop solutions with the observer kernels $m_1(x,\xi)$, $m_2(x,\xi)$, and the control law $U(t)$ given by (55). (b): The closed-loop solutions with the observer kernels $\hat{m}_1(x,\xi)$, $\hat{m}_2(x,\xi)$, and control law $\hat{U}(t)$ given by (115).

7. Concluding remarks

In this paper, we design neural operators for the boundary control of 2 × 2 hyperbolic PDEs system. PDE backstepping-driven DeepONet combines data-driven methods with deductive Lyapunov arguments to expedite the computation of both controller and observer gains exploiting the functional parameters of the plant. Our key results are the *L^2-global exponential stability (GES)* with NO-approximated gain functions and the *semi-global practical exponential stability (SG-PES)* when the observer state is learned and input to the controller.

Acknowledgments

The work of S. Wang was funded by the National Natural Science Foundation of China grant 62303324. The work of M. Diagne was funded by NSF CAREER award CMMI-2302030 and NSF grant CMMI-2222250. The work of M. Krstic was funded by NSF grant ECCS-2151525 and AFOSR grant FA9550-23-1-0535.

References

Anfinsen, H., & Aamo, O. M. (2019). *Adaptive control of hyperbolic PDEs*. Springer.
Anfinsen, H., Diagne, M., Aamo, O. M., & Krstic, M. (2016). An adaptive observer design for $n+1$ coupled linear hyperbolic PDEs based on swapping. *IEEE Transactions on Automatic Control*, *61*(12), 3979–3990.
Anfinsen, H., Diagne, M., Aamo, O. M., & Krstic, M. (2017). Estimation of boundary parameters in general heterodirectional linear hyperbolic systems. *Automatica: A Journal of IFAC the International Federation of Automatic Control*, (79), 185–197.
Bastin, G., & Coron, J.-M. (2010). Further results on boundary feedback stabilisation of 2 × 2 hyperbolic systems over a bounded interval. *IFAC Proceedings Volumes*, *43*(14), 1081–1085.
Bastin, G., & Coron, J.-M. (2011). On boundary feedback stabilization of non-uniform linear 2 × 2 hyperbolic systems over a bounded interval. *Systems & Control Letters*, *60*(11), 900–906.
Bhan, L., Shi, Y., Karafyllis, I., Krstic, M., & Rawlings, J. B. (2024a). Moving-horizon estimators for hyperbolic and parabolic PDEs in 1-D. In *2024 American Control Conference* (pp. 4735–4740). IEEE.
Bhan, L., Shi, Y., & Krstic, M. (2024b). Neural operators for bypassing gain and control computations in PDE backstepping. *IEEE Transactions on Automatic Control*, *69*(8), 5310–5325.
Burkhardt, M., Yu, H., & Krstic, M. (2021). Stop-and-go suppression in two-class congested traffic. *Automatica*, *125*, Article 109381.
Coron, J.-M., D'Andrea-Novel, B., & Bastin, G. (1999). A Lyapunov approach to control irrigation canals modeled by Saint–Venant equations. In *1999 European control conference* (pp. 3178–3183). IEEE.
Deng, B., Shin, Y., Lu, L., Zhang, Z., & Karniadakis, G. E. (2022). Approximation rates of deeponets for learning operators arising from advection-diffusion equations. *Neural Networks*, *153*, 411–426.
Di Meglio, F., Kaasa, G.-O., Petit, N., & Alstad, V. (2012). Model-based control of slugging: advances and challenges. *IFAC Proceedings Volumes*, *45*(8), 109–115.
Di Meglio, F., Vazquez, R., & Krstic, M. (2013). Stabilization of a system of $n+1$ coupled first-order hyperbolic linear PDEs with a single boundary input. *IEEE Transactions on Automatic Control*, *58*(12), 3097–3111.
Di Meglio, F., Vazquez, R., Krstic, M., & Petit, N. (2012). Backstepping stabilization of an underactuated 3 × 3 linear hyperbolic system of fluid flow equations. In *2012 American control conference* (pp. 3365–3370). IEEE.
Diagne, A., Bastin, G., & Coron, J.-M. (2012). Lyapunov exponential stability of 1-D linear hyperbolic systems of balance laws. *Automatica*, *48*(1), 109–114.
Diagne, A., Diagne, M., Tang, S., & Krstic, M. (2017). Backstepping stabilization of the linearized Saint–Venant–Exner model. *Automatica*, *76*, 345–354.
Diagne, M., Tang, S.-X., Diagne, A., & Krstic, M. (2017). Control of shallow waves of two unmixed fluids by backstepping. *Annual Reviews in Control*, *44*, 211–225.
Goatin, P. (2006). The Aw–Rascle vehicular traffic flow model with phase transitions. *Mathematical and Computer Modelling*, *44*, 287–303.
Halleux, J. D., Prieur, C., Coron, J. M., D'Andrea-Novel, B., & Bastin, G. (2003). Boundary feedback control in networks of open channels. *Automatica*, *39*(8), 1365–1376.
Hu, L., Di Meglio, F., Vazquez, R., & Krstic, M. (2016). Control of homodirectional and general heterodirectional linear coupled hyperbolic PDEs. *IEEE Transactions on Automatic Control*, *61*(11), 3301–3314.
Karafyllis, I., Kontorinaki, M., & Krstic, M. (2020). Adaptive control by regulation-triggered batch least squares. *IEEE Transactions on Automatic Control*, *65*(7), 2842–2855.
Krstic, M., Bhan, L., & Shi, Y. (2024). Neural operators of backstepping controller and observer gain functions for reaction–diffusion PDEs. *Automatica*, *164*, Article 111649.
Lamarque, M., Bhan, L., Shi, Y., & Krstic, M. (2025). Adaptive neural-operator backstepping control of a benchmark hyperbolic PDE. *Automatica*, *177*, Article 112329.
Lamarque, M., Bhan, L., Vazquez, R., & Krstic, M. (2025). Gain scheduling with a neural operator for a transport PDE with nonlinear recirculation. *IEEE Transactions on Automatic Control*, http://dx.doi.org/10.1109/TAC.2025.3549700.
Lu, L., Jin, P., & Karniadakis, G. E. (2019). Deeponet: Learning nonlinear operators for identifying differential equations based on the universal approximation theorem of operators. arXiv preprint arXiv:1910.03193.
Qi, J., Zhang, J., & Krstic, M. (2024). Neural operators for PDE backstepping control of first-order hyperbolic PIDE with recycle and delay. *Systems & Control Letters*, *185*, Article 105714.
Somathilake, E., & Diagne, M. (2024). Output feedback control of suspended sediment load entrainment in water canals and reservoirs. *58*, (28), (pp. 983–988).
Vazquez, R., Coron, J.-M., Krstic, M., & Bastin, G. (2012). Collocated output-feedback stabilization of a 2 × 2 quasilinear hyperbolic system using backstepping. In *2012 American control conference* (pp. 2202–2207). IEEE.
Vazquez, R., & Krstic, M. (2014). Marcum q-functions and explicit kernels for stabilization of 2 × 2 linear hyperbolic systems with constant coefficients. *Systems & Control Letters*, *68*, 33–42.

Vazquez, R., Krstic, M., & Coron, J.-M. (2011). Backstepping boundary stabilization and state estimation of a 2 × 2 linear hyperbolic system. In *2011 50th IEEE conference on decision and control and European control conference* (pp. 4937–4942).
Wang, J., & Diagne, M. (2024). Delay-adaptive boundary control of coupled hyperbolic PDE-ODE cascade systems. *IEEE Transactions on Automatic Control*, *69*(12), 8156–8171.
Wang, S., Diagne, M., & Krstic, M. (2023a). Backstepping neural operators for 2 × 2 hyperbolic PDEs. *Automatica*, arXiv preprint arXiv:2312.16762.
Wang, S., Diagne, M., & Krstic, M. (2025). Deep learning of delay-compensated backstepping for reaction–diffusion PDEs. *IEEE Transactions on Automatic Control*, http://dx.doi.org/10.1109/TAC.2025.3538755.
Yu, H., & Krstic, M. (2019). Traffic congestion control for Aw–Rascle–Zhang model. *Automatica*, *100*, 38–51.
Zhang, Y., Zhong, R., & Yu, H. (2024). Neural operators for boundary stabilization of stop-and-go traffic. In *Proceedings of the 6th Learning for Dynamics & Control Conference* (pp. 554–565).

Shanshan Wang is currently a Lecturer (Assistant Professor) at the University of Shanghai for Science and Technology, Shanghai, China. She received the B.S. degree in Electrical Engineering and Automation from Nanhang Jincheng College, Nanjing, China, in 2015, and the Ph.D. degree in control theory and control engineering from Donghua University, Shanghai, China, in 2022. She was a visiting student with the Department of Mechanical Aerospace and Nuclear Engineering at Rensselaer Polytechnic Institute, Troy, New York, from November 2018 to December 2019, and a visiting student with the Chair of Automatic Control, Faculty of Engineering, Kiel University, Kiel, Germany from November 2021 to September 2022. Her research interests include multi-agent cooperative control, the control of delay systems and adaptive control.

Mamadou Diagne is an Associate Professor with the Department of Mechanical and Aerospace Engineering at the University of California San Diego, affiliated with the Department of Electrical and Computer Engineering. He completed his Ph.D. in 2013 at University Claude Bernard Lyon I, Villeurbanne (France). Between 2017 and 2022, he was an Assistant Professor with the Department of Mechanical Aerospace and Nuclear Engineering at Rensselaer Polytechnic Institute, Troy, New York. From 2013 to 2016, he was a Postdoctoral Scholar, first at the University of California San Diego, and then at the University of Michigan. His research focuses on the control of distributed parameter systems (DPS), adaptive control, time-delay systems, extremum seeking control and safe nonlinear control. He served as Associate Editor for Automatica, Systems & Control Letters and ASME Journal of Dynamic Systems, Measurement, and Control. He is Vice-Chair for Industry of the IFAC Technical Committee on Adaptive and Learning Systems and Vice-Chair for Education of the IFAC Technical Committee on Distributed Parameter Systems. He received the NSF Career Award in 2020.

Miroslav Krstic is Distinguished Professor and Senior Associate Vice Chancellor for Research at University of California, San Diego. He is Fellow of IEEE, IFAC, ASME, SIAM, AAAS, AIAA (Assoc. Fellow), IET (UK), and member of the Serbian Academy of Sciences and Arts. Krstic is a recipient of the Bellman Control Heritage Award, Bode Lecture Prize, SIAM Reid Prize, ASME Oldenburger Medal, Nyquist Lecture Prize, Paynter Award, Ragazzini Education Award, IFAC Nonlinear Control Systems Award, IFAC Ruth Curtain Distributed Parameter Systems Award, IFAC Adaptive and Learning Systems Award, Chestnut textbook prize, CSS Distinguished Member Award, the PECASE, NSF Career, and ONR Young Investigator awards, and the Schuck ('96 and '19) and Axelby paper prizes. Krstic is also the inaugural recipient of the A.V. Balakrishnan Award for the Mathematics of Systems. He is due to transition from Editor-in-Chief of Systems & Control Letters to EiC of IEEE Trans. Automatic Control in January 2026. Krstic has coauthored 19 books and about 500 journal papers.